

RSC Advances



This is an *Accepted Manuscript*, which has been through the Royal Society of Chemistry peer review process and has been accepted for publication.

Accepted Manuscripts are published online shortly after acceptance, before technical editing, formatting and proof reading. Using this free service, authors can make their results available to the community, in citable form, before we publish the edited article. This *Accepted Manuscript* will be replaced by the edited, formatted and paginated article as soon as this is available.

You can find more information about *Accepted Manuscripts* in the [Information for Authors](#).

Please note that technical editing may introduce minor changes to the text and/or graphics, which may alter content. The journal's standard [Terms & Conditions](#) and the [Ethical guidelines](#) still apply. In no event shall the Royal Society of Chemistry be held responsible for any errors or omissions in this *Accepted Manuscript* or any consequences arising from the use of any information it contains.

COMMUNICATION

Ultra-High Proton Conduction in Electrospun Sulfonated Polyimide Nanofibers

Cite this: DOI: 10.1039/x0xx00000x

Ryouhei Takemori,^a Genki Ito,^a Manabu Tanaka,^a and Hiroyoshi Kawakami*^a

Received 00th January 2012,

Accepted 00th January 2012

DOI: 10.1039/x0xx00000x

www.rsc.org/

Uniaxially-aligned sulfonated polyimide (SPI) nanofibers fabricated by an electrospinning method showed ultra-high proton conductivities above 1 S cm⁻¹ at 30-90°C and 95%RH. Higher applied voltage between the parallel electrodes during the electrospinning process gave higher proton conductive SPI nanofibers due to the formation of effective proton conduction pathway by molecular orientation in the nanofibers.

Polymer electrolyte fuel cell directly converts chemical energy into electrical energy with a high efficiency and low emission of pollutants, and is one of the most promising power sources for portable, stationary, and automotive applications.¹ Proton exchange membrane (PEM), a key component in fuel cell systems, requires high proton conductivity, low gas permeability, and chemical stabilities.² Perfluorosulfonated membranes such as Nafion have been widely used because of their excellent oxidative and hydrolysis stability as well as high proton conductivity.³ Recently several researches have indicated that scaling down Nafion to the nanometer size scale may impact its properties and subsequently its performance in devices. For example, Nafion nanofibers prepared through an electrically charged jet of a polymer solution (electrospinning) have shown unique properties. Snyder and Elabd reported on the improvement of fuel cell performance due to electrospun Nafion nanofibers that form in fuel cell electrodes.⁴ Zhu and co-workers demonstrated improved fuel cell performance with a Nafion nanofiber-based fuel cell.⁵ Other researchers also reported on the benefits of Nafion nanofibers in fuel cells.⁶ Recently, proton conductivity of a single Nafion nanofiber with 400 nm diameter was measured to be 1.5 S cm⁻¹ at 30°C and 90%RH, which is an order of magnitude higher than the bulk Nafion film (~0.1 S cm⁻¹).⁷ However, these nanofibers have not been fabricated from the pure Nafion because of its too low polymer chain entanglement in solvents to form nanofibers by the electrospinning method. Therefore, high molecular weight poly(ethylene oxide) or poly(vinyl alcohol) was required as a spinning aid to give Nafion nanofibers. Besides, Nafion and other perfluorosulfonated ionomer membranes have limitations on their high cost, low thermal stability due to their low T_g , and low gas barrier properties for future fuel cell applications.

For past decades, much effort has gone into the development of novel polymer electrolyte membranes based on the sulfonated aromatic hydrocarbon polymers, which have been widely synthesized as alternate candidates due to their excellent chemical, thermal, and mechanical stabilities.⁸ Recently, Pintauro and Mather attempted sulfonated aromatic hydrocarbon polymer nanofibers to PEMs to achieve better gas barrier properties and to prevent from undesirable membrane swelling.⁹ We also reported that sulfonated polyimide (SPI) nanofibers-containing PEMs showed distinguished gas barrier properties and chemical stabilities.¹⁰ Furthermore, the membrane containing uniaxially-aligned SPI nanofibers showed higher in-plane proton conductivity along the fiber direction than the corresponding SPI membrane prepared by a conventional solvent cast method.^{10(a),(c)} Though enhancement of through-plane proton conductivity of the nanofiber composite membrane is still challenging, the composite membrane showed better fuel cell performances due to its lower fuel crossover than the corresponding membranes without nanofibers.^{10(a)} Similar improvement of fuel cells by using nanofiber-containing composite membranes have been reported by several groups.¹¹ However, the properties of sulfonated aromatic hydrocarbon polymers on the nanoscale, such as intrinsic proton conductivity of the nanofibers, have not yet been addressed. Elucidation of the intrinsic proton conductivity on the electrospun polymer nanofibers and construction of optimal three-dimensional assembled structures with appropriate nanofibers will achieve novel polymer electrolyte membranes containing proton conductive polymer nanofibers with high through-plane proton conductivity.

Here we first report the intrinsic proton conductive characteristics of sulfonated aromatic hydrocarbon polymer nanofibers. Uniaxially-aligned SPI nanofibers fabricated between two parallel collector electrodes were prepared by an electrospinning method, and their proton conductivities were measured at various temperatures and humidity. The orientation of polymer chains in the nanofibers were studied by attenuated total reflectance Fourier transform infrared spectroscopy (ATR FT-IR) through a polarizer. We revealed that the applied voltage between the parallel electrodes during the electrospinning process affected on the proton conductivity of the SPI nanofibers because of the difference in molecular orientation in the electrospun SPI nanofibers.

The sulfonated polyimide (SPI: 6FDA-BDSA-*r*-APPF, $M_w = 3.4 \times 10^5$, $M_w/M_n = 1.8$, Fig. 1) was obtained by imidation of the

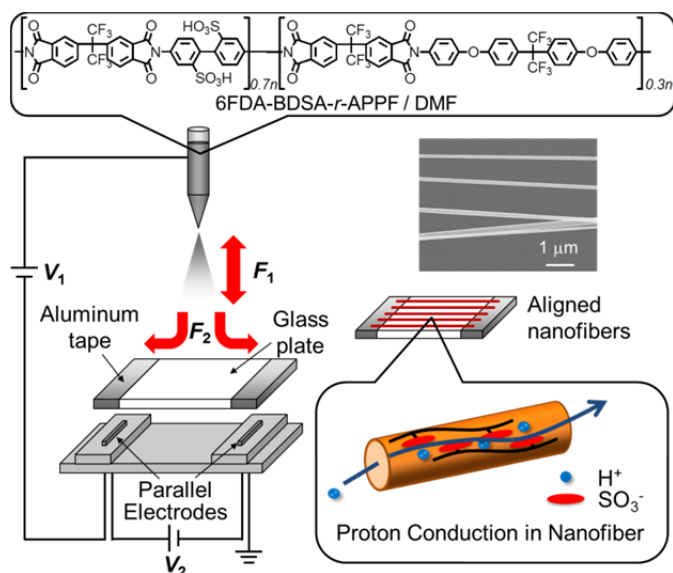


Fig. 1 Schematic illustration of SPI (6FDA-BDSA-*r*-APPF) nanofibers: Preparation and proton conductivity measurement.

precursor poly(amic acid) in the presence of benzoic acid and triethylamine as described in our previous paper.^{10(c)} Ion exchange capacity (IEC) of the SPI in a proton form was determined to be 1.65 meq g⁻¹. The polymer structure and IEC values in this study were chosen in consideration of its proton conductivity, chemical stability, and nanofiber formability based on our previous study.¹⁰ The SPI nanofibers were prepared by the electrospinning, which is a method of discharging a polymer solution in air from a spinneret onto grounded plate collector under high voltage (V_1) to produce nanofibers by exploiting electrostatic repulsion (F_1) of the polymer solution (Fig. 1). In order to prepare uniaxially-aligned nanofibers, parallel aluminum electrodes on glass plate were used as a grounded collector where another high voltage (V_2) can be applied between the parallel electrodes. The uniaxially-aligned nanofibers were deposited on the glass plate to bridge the two parallel electrodes by means of electrostatic attractive force (F_2) between the parallel electrodes. The size and morphology of electrospun uniaxially-aligned nanofibers were controlled by the electrospinning conditions.¹² A typical SEM image of the uniaxially-aligned electrospun SPI nanofibers are also shown in Figure 1. The image clearly demonstrated that the uniform nanofibers with smooth surfaces were almost uniaxially-aligned and were individually deposited across the gap between the aluminum electrodes. It is considered that the electrostatic forces formed between the charged nanofiber and the aluminum electrode determined the uniaxially-aligned direction of the nanofibers. Average diameters of the electrospun SPI nanofibers prepared by different V_2 voltages were calculated to be 223±43, 145±29, and 108±22 nm when the V_2 were 0.5, 1.0 and 3.0 kV, respectively (Table 1, Fig. S1 in ESI†).

The proton conductivities of SPI membranes and nanofibers, which were treated in advance with hydrochloric acid to be proton forms, were measured by an electrochemical impedance spectroscopy. Intrinsic proton conductivity (σ) of the nanofibers were determined from the following equation; $\sigma = d/(a \cdot N \cdot R)$, where R , a , N , and d are impedance value, cross-sectional area of a single nanofiber, numbers of uniaxially-aligned nanofibers between the electrodes, and distance between the electrodes, respectively, by reference to the proton conductivity measurement of conventional polymer electrolyte membranes ($\sigma = d/(A \cdot R)$, where A is conducting area calculated from thickness and width of the membrane). Typical

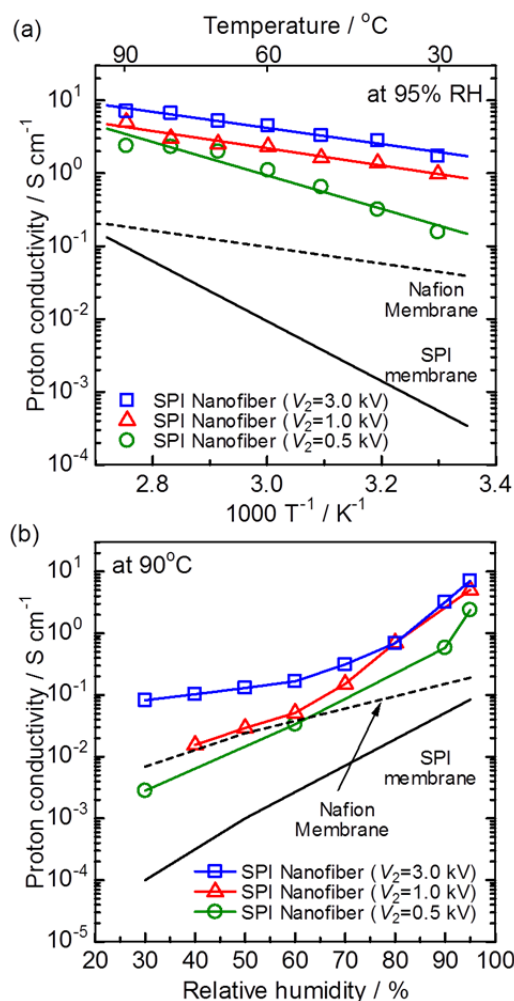


Fig. 2 (a) Temperature dependence (at 95%RH) and (b) relative humidity dependence (at 90°C) of proton conductivity of the SPI nanofibers prepared from different electrospinning condition ($V_2 = 0.5, 1.0,$ and 3.0 kV), the SPI cast membrane, and the Nafion membrane.

Nyquist plots of impedance measurement on the SPI nanofibers ($V_2 = 3.0$ kV) are shown in Fig. S2 in ESI†.

Fig. 2 (a) shows the proton conductivities of SPI nanofibers prepared by electrospinning under different V_2 conditions ($V_2 = 0.5, 1.0,$ or 3.0 kV) as a function of temperature at 95%RH. The proton conductivities of SPI and Nafion 117 membranes were also depicted by way of comparison. The proton conductivities of the SPI nanofibers were two orders higher than those of corresponding SPI membranes at all the temperature ranges. This tendency that electrospun nanofibers have higher proton conductivity than the corresponding membrane coincides with the results of Nafion nanofibers and membranes reported before.⁷ The activation energies (E_a) of the proton conductivity on the SPI nanofibers (21 - 44 kJ mol⁻¹) were obviously lower than that of the SPI membrane (79 kJ mol⁻¹) as summarized in Table 1. It is considered that the electrospun polymer nanofibers may have better proton conduction pathway than the cast membranes. Fig. 2(b) represents relative humidity dependences of the proton conductivities. The proton conductivities of the SPI nanofibers decreased with decreasing relative humidity, indicating the proton conduction in the nanofibers are also classified to the Vehicle Mechanism where protons transport with mediating with water molecules. However, the SPI nanofibers maintained higher proton conductivities than the SPI membrane and were comparable to Nafion membrane even at low relative humidities.

COMMUNICATION

Table 1. Proton conductivities and activation energies of the uniaxially-aligned SPI nanofibers prepared from different electrospinning conditions, the SPI membrane, and Nafion membrane.

| run | sample | V_2 (kV) | Fiber diameter (nm) | Proton conductivity (S/cm) | | | | E_a (kJ/mol) |
|-----------------|-----------------|------------|---------------------|----------------------------|----------------------|----------------------|------------------------------------|----------------|
| | | | | 30°C, 95%RH | 60°C, 95%RH | 90°C, 95%RH | 90°C, 30%RH | |
| 1 ^{b)} | | 3.0 | 108±22 | 1.7×10^0 | 4.5×10^0 | 7.1×10^0 | 8.2×10^{-2} | 21 |
| 2 ^{b)} | SPI nanofibers | 1.0 | 145±29 | 9.8×10^{-1} | 2.3×10^0 | 5.1×10^0 | 1.6×10^{-2} ^{d)} | 23 |
| 3 ^{b)} | | 0.5 | 223±43 | 1.6×10^{-1} | 1.1×10^0 | 2.4×10^0 | 2.8×10^{-3} | 44 |
| 4 ^{c)} | | 0.5 | 146±28 | 4.3×10^{-1} | 8.7×10^{-1} | 7.4×10^0 | 1.2×10^{-2} | 42 |
| 5 | SPI membrane | - | - | 5.4×10^{-4} | 4.0×10^{-2} | 8.3×10^{-2} | 1.0×10^{-4} | 79 |
| 6 | Nafion membrane | - | - | 4.8×10^{-2} | 9.5×10^{-2} | 1.9×10^{-1} | 6.9×10^{-3} | 22 |

a) Activation energy of proton conductivity at 95%RH, b) All electrospinning conditions were same except V_2 voltages, c) Electrospinning conditions were tuned to give nanofibers with ca. 145 nm-diameter with keeping V_2 voltages to 0.5 kV, d) at 90°C, 40%RH.

Besides, the SPI nanofibers showed unique relative humidity dependency of proton conductivity, that is to say, the conductivity drops of the SPI nanofibers, especially the nanofibers prepared at $V_2 = 3.0$ kV, under low relative humidity conditions were smaller than that of the SPI membrane. In order to compare the amounts of water between the nanofibers and the membrane, water uptakes of the SPI membrane and the SPI nanofibers (nanofibrous membrane) were measured as a function of relative humidity (Figure S3 in ESI†). Interestingly, the SPI nanofibers showed higher water uptake than the SPI membrane at low relative humidity. Such relatively high water retention in the nanofibers at low relative humidity suggests remarkable continuous hydrophilic proton conductive channels in the nanofibers. It may be originated from the hydrophilic/hydrophobic phase separation in the nanofibers during the electrospinning process,^{10(a)} leading suppressed conductivity drops in the SPI nanofibers at low relative humidity.

It is noteworthy that the SPI nanofibers prepared from different electrospinning conditions ($V_2 = 0.5, 1.0,$ or 3.0 kV) showed distinct differences on their proton conductivities as shown in Fig. 2. The SPI nanofibers prepared from higher V_2 voltages showed higher proton conductivity and lower activation energy (Table 1). It is thought to be due to the following two reasons: First, nanofiber diameters would affect their proton conductivities. Protons could rectilinearly transport faster in a thinner nanofiber because of its quasi-one-dimensional narrow conduction pathway. The previous study on proton conductivity of Nafion nanofibers also revealed that the proton conductivity increased sharply with decreasing fiber diameter.⁷ Secondly, molecular orientation in the electrospun nanofibers should have influence on their proton conductivities. Polymer nanofibers prepared from the electrospinning process are known to possess a distinguishing characteristic, *i.e.* super molecular arrangement effect, which leads to greater thermal stability, higher mechanical toughness, and faster material transport.¹³ For example, in the case of electrical conductive PEDOT:PSS-PVA nanofibers, it was reported the electrical conductivity of the nanofibers became altered by changing molecular orientation in the nanofibers.¹⁴ Similar enhancement of material transport was also reported in stretched membranes where molecular orientation were induced along extended axis. Allahyarov and Taylor have revealed

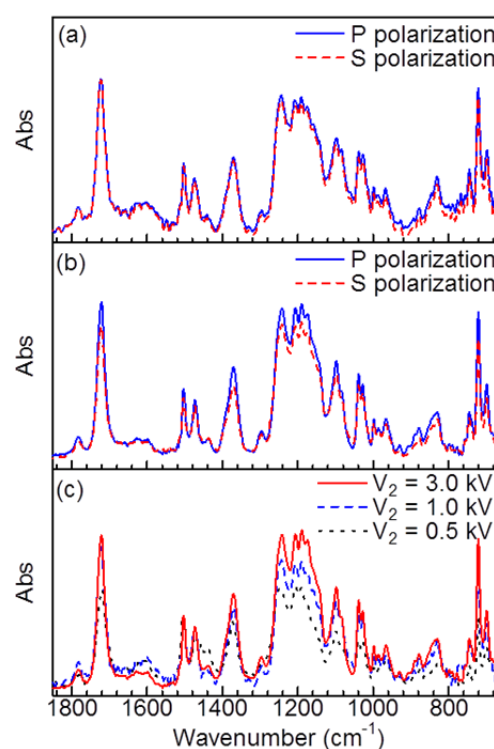


Fig. 3 The polarized ATR FT-IR spectra of (a) the SPI cast membrane, (b) the uniaxially-aligned SPI nanofibers prepared from V_2 voltage of 3.0 kV, and (c) P polarization spectra of the uniaxially-aligned SPI nanofibers prepared from different electrospinning conditions ($V_2 = 0.5, 1.0,$ and 3.0 kV).

correlation between structure and proton conductivity of stretched Nafion membrane.¹⁵

In order to investigate molecular orientation in SPI nanofibers, polarized ATR FT-IR spectroscopy was used. Measurements and peak assignments were made on four different samples – a SPI cast membrane and three types of uniaxially-aligned SPI nanofibers prepared from different V_2 voltages including 3.0, 1.0, and 0.5 kV. The polarized ATR FT-IR spectra of the SPI cast membrane are shown in Fig. 3(a), and the typical peaks are well-assigned to the SPI

structure (see ESI†). It stands to reason that spectral configuration and peak intensities of the SPI membrane for the polarized measurements with parallel axis (P polarization) are equivalent to those with perpendicular axis (S polarization), since the SPI membrane was amorphous and had no anisotropy. On the other hand, uniaxially-aligned SPI nanofibers indicated different results. The peak intensities for polarized measurements parallel to fiber axis (P polarization) were greater compared to those from the perpendicular measurements (S polarization) as shown in Fig. 3(b). The difference in the absorbance intensities between parallel and perpendicular polarization can be attributed to molecular orientation of the polymer backbone in the nanofibers. It is normally observed that intensity of P polarization is higher than that of S polarization when the polymer backbone orients along the nanofiber axis;¹⁶ therefore, the results in Fig. 3(b) demonstrates the molecular orientation of SPI backbone along the nanofibers. Fig. 3(c) represents the P polarization spectra of uniaxially-aligned SPI nanofibers prepared from V_2 voltages of 3.0, 1.0, and 0.5 kV. The peak intensities for the uniaxially-aligned SPI nanofibers became greater with increasing V_2 voltages, meaning that higher V_2 voltages gave nanofibers with higher molecular orientation due to electrostatic attractive force between two parallel electrodes.

The polarized ATR FT-IR spectroscopy supported the proton conductivity enhancement in the uniaxially-aligned SPI nanofibers, especially in the nanofibers prepared from higher V_2 voltages, due to the effect of molecular orientation in the nanofibers. However, as shown in Table 1 run 1-3, higher V_2 voltages led thinner fiber diameters that would also effect on proton conductivity of the SPI nanofibers described above. Hence finally, to make clear the influence of V_2 voltages and accompanying molecular orientation of the SPI nanofibers on their proton conductivities, uniaxially-aligned SPI nanofibers with similar fiber diameters were prepared from different V_2 voltages by tuning other electrospinning parameters (Table 1 run 4). The uniaxially-aligned SPI nanofibers with 146 ± 28 nm diameters, which were almost equal to the SPI nanofibers with 145 ± 29 nm diameters from the V_2 voltage of 1.0 kV (run 2), were prepared from the V_2 voltage of 0.5 kV (run 4). As is apparent from Table 1, the uniaxially-aligned SPI nanofibers (146 ± 28 nm diameter, $V_2 = 0.5$ kV) showed lower proton conductivity than the nanofibers (146 ± 28 nm diameter, $V_2 = 1.0$ kV) at low relative humidity or low temperature. The activation energy of proton conductivity on the SPI nanofibers (146 ± 28 nm diameter, $V_2 = 0.5$ kV, run 4) was close to that on the SPI nanofibers (223 ± 43 nm diameter, $V_2 = 0.5$ kV, run 3), suggesting the V_2 voltage and accompanying molecular orientation of the SPI nanofibers are more effective on the proton conductivity than the diameter of nanofibers.

In conclusion, we have succeeded in evaluating proton conductivity of the uniaxially-aligned SPI nanofibers prepared by the electrospinning method using two parallel collector electrodes. Proton conductivity of the SPI nanofibers was higher than that of the corresponding SPI membrane. Besides, it was revealed that the SPI nanofibers prepared from higher V_2 voltage between the parallel electrodes showed higher proton conductivity. The polarized ATR FT-IR supported the molecular orientation of the polymer backbone along the nanofiber axis enhanced the proton conductivity in the SPI nanofibers due to the formation of better proton conduction pathway. Elucidation of the intrinsic proton conductivity on the electrospun polymer nanofibers will help for molecular design of high-performance polymer electrolyte membranes containing proton conductive polymer nanofibers for future fuel cell applications.

This work was partially supported by a grant (No.08004961-0) from NEDO, a grant (ACLA) from JST, and JSPS KAKENHI Grant Number 24750225.

Notes and references

^a Department of Applied Chemistry, Tokyo Metropolitan University, Hachioji, Tokyo 192-0397, Japan, Fax: (+) 81-426-77-2821, E-mail: kawakami-hiroyoshi@tmu.ac.jp

† Electronic Supplementary Information (ESI) available: Experimental methods, SEM images of the nanofibers, typical Nyquist plots, water uptakes, and FT-IR peak assignment. See DOI: 10.1039/c000000x/

- (a) W. Vielstich, *Handbook of Fuel Cells*, Wiley, Chichester, England, 2009; (b) L. Carrette, K. A. Friedrich, and U. Stimming, *Fuel Cells*, 2001, **1**, 5; (c) R. Borup, J. Meyers, B. Pivovar, Y.-S. Kim, R. Mukundan, N. Garland, D. Myers, M. Wilson, F. Garzon, D. Wood, P. Zelenay, K. More, K. Stroh, T. Zawodzinski, J. Boncella, J. E. McGrath, M. Inaba, K. Miyatake, M. Hori, K. Ota, Z. Ogumi, S. Miyata, A. Nishikata, Z. Siroma, Y. Uchimoto, K. Yasuda, K. Kimijima, and N. Iwashita, *Chem. Rev.*, 2007, **107**, 3904.
- (a) B. C. Steele and A. Heinzl, *Nature*, 2001, **414**, 345; (b) J. Rozière and D. J. Jones, *Annu. Rev. Mater. Res.*, 2003, **33**, 503; (c) M. A. Hickner and B. S. Pivovar, *Fuel Cells*, 2005, **5**, 213.
- (a) M. W. Verbrugge and R. F. Hill, *J. Electrochem. Soc.*, 1990, **137**, 3770; (b) K. S. Rohr and Q. Chen, *Nat. Mater.*, 2008, **7**, 75.
- J. D. Snyder and Y. A. Elabd, *J. Power Sources*, 2009, **186**, 385.
- C. Pan, H. Wu, C. Wang, B. Wang, L. Zhang, Z. Cheng, P. Hu, W. Pan, Z. Zhou, X. Yang, and J. Zhu, *Adv. Mater.*, 2008, **20**, 1644.
- J. B. Ballengee and P. N. Pintauro, *Macromolecules*, 2011, **44**, 7307.
- B. Dong, L. Gwee, D. Salas-de la Cruz, K. I. Winey, and Y. A. Elabd, *Nano Lett.*, 2010, **10**, 3785.
- (a) Z. Hu, Y. Yin, K. Yaguchi, N. Endo, M. Higa, and K. Okamoto, *Polymer*, 2009, **50**, 2933; (b) J. Saito, M. Tanaka, K. Miyatake, and M. Watanabe, *J. Polym. Sci. Polym. Chem.*, 2010, **48**, 2846; (c) S. Seesukphronrarak, K. Ohira, K. Kidena, N. Takimoto, C. S. Kuroda, and A. Ohira, *Polymer*, 2010, **51**, 623; (d) K. Xu, H. Oh, M. A. Hickner, and Q. Wang, *Macromolecules*, 2011, **44**, 4605; (e) K. Yamazaki, G. Wang, M. Tanaka, and H. Kawakami, *J. Power Sources*, 2012, **216**, 387; (f) K. Suzuki, Y. Iizuka, M. Tanaka, and H. Kawakami, *J. Mater. Chem.*, 2012, **22**, 23767; (g) B. Campagne, G. David, B. Améduri, D. J. Jones, J. Rozière, and I. Roche, *Macromolecules*, 2013, **46**, 3046.
- (a) J. Choi, K. M. Lee, R. Wycisk, P. N. Pintauro, and P. T. Mather, *Macromolecules*, 2008, **41**, 4569; (b) J. Choi, K. M. Lee, R. Wycisk, P. N. Pintauro, and P. T. Mather, *J. Electrochem. Soc.*, 2010, **157**, B914.
- (a) T. Tamura and H. Kawakami, *Nano Lett.*, 2010, **10**, 1324; (b) R. Takemori and H. Kawakami, *J. Power Sources*, 2010, **195**, 5957; (c) T. Tamura, R. Takemori, and H. Kawakami, *J. Power Sources*, 2012, **217**, 135.
- (a) J. Choi, K. M. Lee, R. Wycisk, P. N. Pintauro, and P. T. Mather, *J. Mater. Chem.*, 2010, **20**, 6282; (b) S. Mollá, V. Compañ, E. Gimenez, A. Blazquez, and I. Urdanpilleta, *Int. J. Hydrogen Energy*, 2011, **36**, 9886; (c) J. B. Ballengee and P. N. Pintauro, *Macromolecules*, 2011, **44**, 7307.
- Y. Karube and H. Kawakami, *Polym. Adv. Technol.*, 2010, **21**, 861.
- (a) Y. Dzenis, *Science*, 2004, **304**, 1917; (b) V. Thavasi, G. Singh, and S. Ramakrishna, *Energy Environ. Sci.*, 2008, **1**, 205; (c) D. H. Reneker and A. L. Yarin, *Polymer*, 2008, **49**, 2387; (d) Y.-Z. Long,

Journal Name

- M.-M.Li, C. Gu, M. Wan, J. L. Duvail, Z. Liu, and Z. Fan, *Prog. Polym. Sci.*, 2011, **36**, 1415.
- 14 N. Liu, G. Fang, J. Wan, H. Zhou, H. Long, and X. Zhao, *J. Mater. Chem.*, 2011, **21**, 18962.
- 15 E. Allahyarov and P. L. Taylor, *J. Phys. Chem. B*, 2009, **113**, 610.
- 16 M. V. Kakade, S. Givens, K. Gardner, K. H. Lee, D. B. Chase, and J. F. Rabolt, *J. Am. Chem. Soc.*, 2007, **129**, 2777.